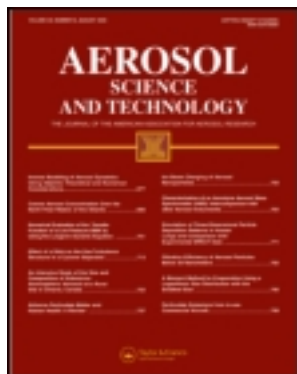


This article was downloaded by: [University Of Maryland]

On: 15 May 2013, At: 15:05

Publisher: Taylor & Francis

Informa Ltd Registered in England and Wales Registered Number: 1072954 Registered office: Mortimer House, 37-41 Mortimer Street, London W1T 3JH, UK



## Aerosol Science and Technology

Publication details, including instructions for authors and subscription information:

<http://www.tandfonline.com/loi/uast20>

### Wavelength-Resolved UV Photoelectric Charging Dynamics of Nanoparticles: Comparison of Spheres and Aggregates

Lei Zhou<sup>a</sup>, Rian You<sup>a</sup>, Jiaojie Tan<sup>a</sup> & Michael R. Zachariah<sup>a</sup>

<sup>a</sup> Department of Mechanical Engineering and Department of Chemistry and Biochemistry, University of Maryland, College Park, Maryland, USA

Accepted author version posted online: 01 Mar 2013. Published online: 27 Mar 2013.

To cite this article: Lei Zhou, Rian You, Jiaojie Tan & Michael R. Zachariah (2013): Wavelength-Resolved UV Photoelectric Charging Dynamics of Nanoparticles: Comparison of Spheres and Aggregates, *Aerosol Science and Technology*, 47:6, 672-680

To link to this article: <http://dx.doi.org/10.1080/02786826.2013.779630>

PLEASE SCROLL DOWN FOR ARTICLE

Full terms and conditions of use: <http://www.tandfonline.com/page/terms-and-conditions>

This article may be used for research, teaching, and private study purposes. Any substantial or systematic reproduction, redistribution, reselling, loan, sub-licensing, systematic supply, or distribution in any form to anyone is expressly forbidden.

The publisher does not give any warranty express or implied or make any representation that the contents will be complete or accurate or up to date. The accuracy of any instructions, formulae, and drug doses should be independently verified with primary sources. The publisher shall not be liable for any loss, actions, claims, proceedings, demand, or costs or damages whatsoever or howsoever caused arising directly or indirectly in connection with or arising out of the use of this material.



# Wavelength-Resolved UV Photoelectric Charging Dynamics of Nanoparticles: Comparison of Spheres and Aggregates

Lei Zhou, Rian You, Jiaojie Tan, and Michael R. Zachariah

*Department of Mechanical Engineering and Department of Chemistry and Biochemistry,  
University of Maryland, College Park, Maryland, USA*

---

The objective of this work is to understand the charging dynamics of metal nanoparticles under wavelength-selected UV irradiation, with a particular focus on the effect of particle structure on the quantum yield. We employed an ion mobility analysis technique to measure the size-resolved single charging efficiency of structure-controlled silver nanoparticles (spheres vs. aggregates) in the mobility diameter ( $D_m$ ) range of 10 ~ 100 nm. We found that the measured particle charging efficiency follows  $D_m^2$  dependence for both spherical and aggregate particles. Based on the measured charging efficiency and calculated particle photon absorption cross section, we are also able to determine the mobility size dependence of photoelectric quantum yield for both spheres and aggregates. The quantum yield of spheres is a constant for larger particles (50 nm or larger) but significantly enhanced as particle size decreases. The quantum yield of aggregates is shown to be particle structure dependent and does not behave as a simple summation of individual primary particles. The aggregate particles have higher quantum yield compared with spheres of the same mobility size but is offset by the lower photon absorption cross section, and thus overall charging efficiency of aggregates is lower than spheres of the same mobility size.

---

[Supplementary materials are available for this article. Go to the publisher's online edition of *Aerosol Science and Technology* to view the free supplementary files.]

## 1. INTRODUCTION

Efficient particle charging is a nontrivial topic faced by a broad range of applications including fabrication of nanoparticle-based devices, property-tailored nanoparticle synthesis, or particle control and filtration (Shimada et al. 1997;

---

Received 21 September 2012; accepted 23 October 2012.

This work was supported by AFOSR—ARAA funding. The authors acknowledge the support of the Maryland NanoCenter and its NispLab. The authors also want to thank Dr. George Mulholland for useful discussions.

Address correspondence to Michael R. Zachariah, Department of Mechanical Engineering and Department of Chemistry and Biochemistry, University of Maryland, 2125 Martin Hall, College Park, MD 20742, USA. E-mail: mrz@umd.edu

Jung and Kittelson 2005; Tsai et al. 2005; Lall et al. 2006). It is particularly critical in aerosol particle instrumentation, where having a well-defined particle charge distribution (particle charging) is essential for subsequent particle manipulation and classification. Currently the vast majority of particle charging devices, such as the “neutralizer” or corona discharger, are based upon diffusion charging because the charging process is generally material independent, and the theories of diffusion charging dynamics in terms of particle size, morphology, etc., are predictable and well understood (Fuchs 1963; Lall et al. 2006; Shin et al. 2010). However, diffusion chargers suffer from relatively low charging efficiency, particularly for small particles. To overcome the charging efficiency limitation, photoelectric ionization charging has been proposed as an alternative approach (Jiang et al. 2007; Hontanon and Kruis 2008). In fact, understanding the photoelectric ionization properties of small particles is not only important in aerosol technology but also crucial from a basic research prospective. It provides a probe of the electronic structure, and the surface activities of nanomaterials and offers one of the direct windows to view the transition of properties from atoms to bulk materials. Typically studies on surface properties of nanoparticles have been limited to samples residing on a surface, but interactions between substrate and particles may severely alter the properties of the nanoparticles and may not represent their intrinsic surface characteristics (Keller et al. 2001; Weber et al. 2001). A variety of cluster beam systems have been developed to probe the photoelectric behavior but such techniques usually require highly sophisticated and specialized facilities (Reiners and Haberland 1996; Wong et al. 2001). So-called aerosol-based techniques, on the other hand, have the advantage that particles are produced and manipulated in a gas stream, and therefore their native properties can be investigated at atmospheric pressure in an on-the-fly size-resolved manner without the interference from a substrate (Schmidt-Ott et al. 1980; Burtscher et al. 1982; Muller et al. 1988; Matter et al. 1995; Weber et al. 2001; Maisels et al. 2002).

There have been several experimental and theoretical efforts to investigate aerosol photoelectric charging dynamics. As photoelectric behavior is an intrinsic property of the material,

photoelectric charging is strongly dependent upon particle composition. Unusual photoelectric activities of ultrafine aerosol particles have been observed for particles less than  $\sim 10$  nm in diameter as compared with the bulk surface (Schmidt-Ott et al. 1980). Dramatic enhancement has been found for variety of metal particles such as Ag, Pd, Cu, and Au, which suggests that the yield enhancement is not a property of the material but a result of quantum particle size effects (Schleicher et al. 1993). In addition to the photoelectron yield, particle work function is also found to be size dependent which is attributed to the image and coulomb potential of a sphere (Wood 1981).

In these reported aerosol-based approaches, particles in the aerosol phase are irradiated by UV light, and the resulting charged particles are examined either by electrometers or through electrical mobility analysis. However the process can be significantly more complex due to simultaneous diffusion charging from negative ions which may co-exist depending on system parameters such as type of carry gas, irradiation intensity, and particle concentration, and thus the resulting particles charge state can be either bipolarly or unipolarly distributed (Matter et al. 1995; Maisels et al. 2002, 2003; Jiang et al. 2007; Hontanon and Kruis 2008). Other effects, such as particle shape are known to have a significant effect on diffusion charging (Oh et al. 2004; Lall et al. 2006; Shin et al. 2010), but have not as yet been evaluated for photoelectric charging.

Recently we employed ion mobility characterization to measure the work function and photoelectric activity of structure-

controlled nanoparticles by UV photoelectric ionization in free flight (Zhou and Zachariah 2011). We found that the Fowler–Nordheim law is applicable to not only spheres but also aggregates. The measured work function of spheres is size dependent and consistent with classical image and coulomb potentials explanations. On the other hand, the measured work function of aggregates is essentially a constant value and only dependent on the primary particle size. In this article, we continue our discussion on the ion mobility measurement results and focus our attention to investigate the single-particle charging dynamics from photoelectric ionization.

## 2. EXPERIMENTAL APPROACH AND DATA EVALUATION

### 2.1. Experimental Setup

The experiment system consists of three components: preparation of structure-controlled neutral silver particles, exposure of polydisperse silver particles to the wavelength-selected UV light for photoelectric particle charging, and finally measurement of the mobility spectrum of charged particles. A schematic of the experimental system is shown in Figure 1.

Silver was chosen in this study because its photoelectric behavior has been well studied and the structure of the silver nanoparticle can be easily controlled. A two-furnace setup was used to generate aggregate or spherical silver nanoparticles. Silver aggregates were generated by heating bulk silver powder

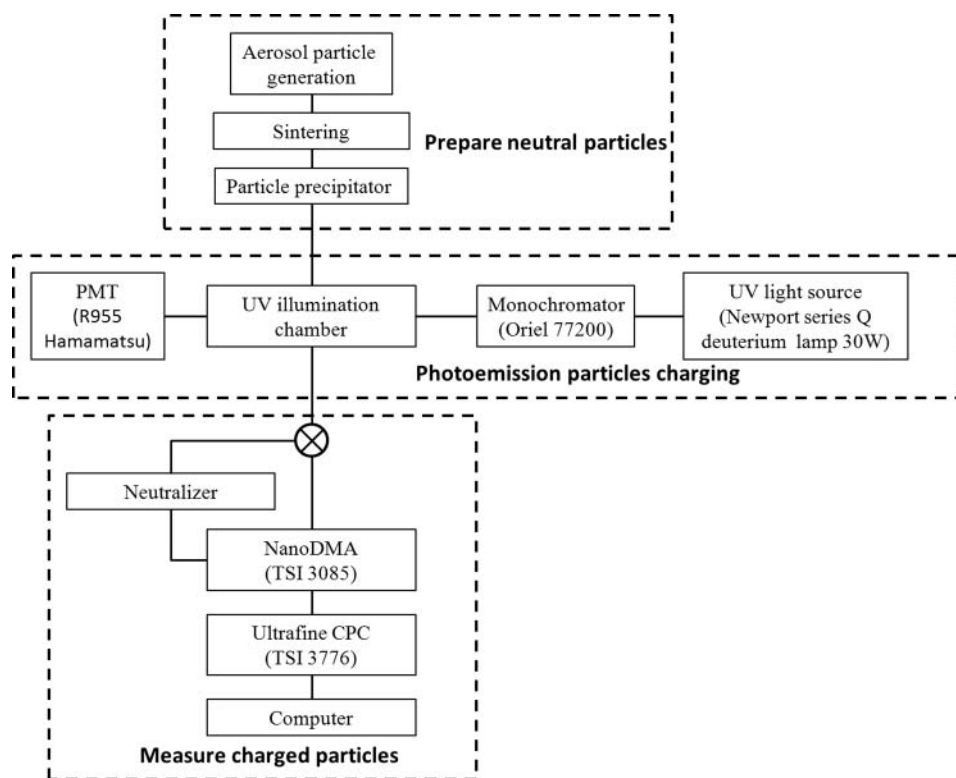


FIG. 1. Schematic of experimental system to measure charging efficiency and work function. (Reprinted from Zhou and Zachariah 2011 with permission from Elsevier.)

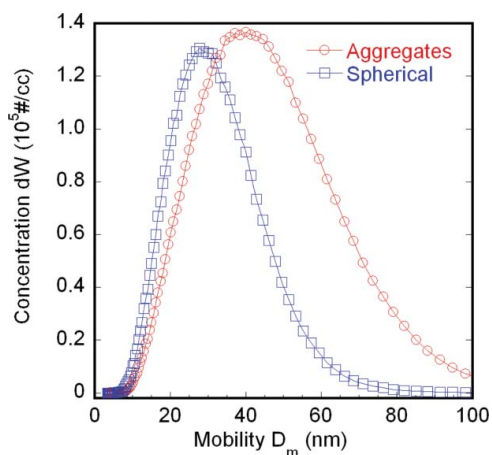


FIG. 2. Particle size distributions of neutral aggregates and sintered spherical silver nanoparticles. (Color figure available online.)

crystal (Alfa Aesar, Ward Hill, MA, USA; 99.9%) in ceramic boat inside a tube furnace at 1050°C in a flow of ultrahigh purity nitrogen. To produce spherical silver particles, the aggregates were sintered in a second furnace at 600°C. Silver particles were then passed through an electrostatic precipitator to remove any pre-existing remnant charged particles. The remaining neutral particles were sent to the photoelectric ionization chamber and exposed to UV irradiation. Figure 2 shows the particle mobility size distribution ( $D_m$ ) of neutral aggregates and sintered particles measured by the nano differential mobility analyzer (NanoDMA TSI 3085; TSI Inc., St. Paul, MN, USA). The aggregate silver particles have a peak mobility size of  $\sim 39$  nm with the total particle concentration of  $\sim 3.2 \times 10^6$  #/cc. Upon sintering the particle peak mobility size shifted to  $\sim 27$  nm indicating a change in particle structure. The morphology of aggregate particles was further examined through transmission electron microscopy (TEM), shown in Figure 3a (not with differential mobility analyzer [DMA] size selection). Based on the TEM image as well as our previous work on aggregate particle work function, we determined that the primary particle in aggregates is about 15 nm (Zhou and Zachariah 2011). Size-resolved sintered (spherical) silver particles were also examined through TEM as shown in Figure 2b. In this TEM measurement, particles of 28.5 nm were selected by the DMA, with a TEM measured average particle size of 28.6 nm (based on a total of 139 particles).

The photoelectric ionization chamber is a 65-cm-long grounded metal tube with i.d. 3.5 cm. For the nominal flow rate of 1 LPM flow rate the particle residence time is estimated to be  $\sim 29$  s. The tube was fully illuminated with a collimated 3.4 cm dia UV beam produced from a 30 W deuterium lamp (Newport series Q, Stamford, CT, USA) coupled with a monochromator (Oriel 77200, Stamford, CT, USA), with the beam intensity measured by a photomultiplier tube (PMT; Hamamatsu R955, Middlesex, NJ, USA). In the experiment, a total of nine wavelength bands ranging from 200 to 280 nm (photon energy 6.20–4.43 eV) were selected by the monochromator to photoionize particles, and the mobility spectrum of the resulting

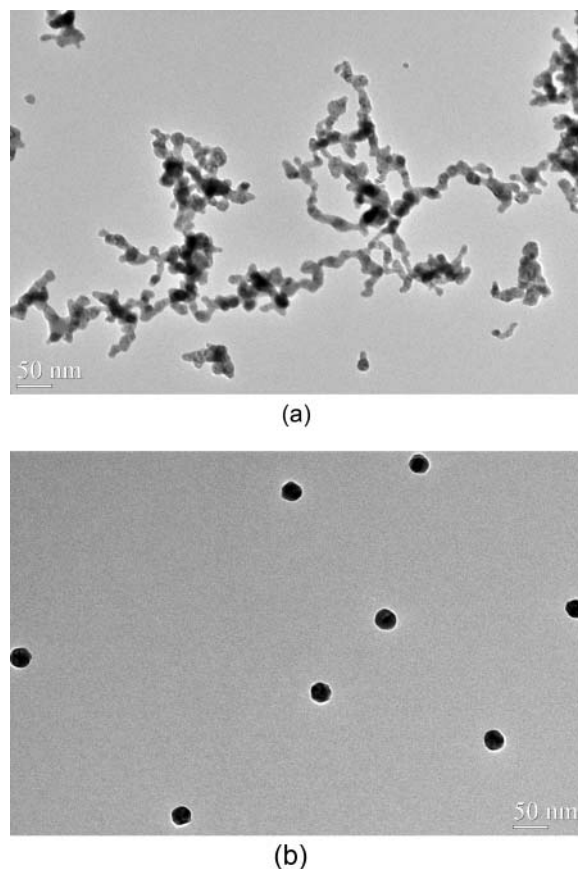


FIG. 3. TEM images of (a) aggregate silver particles (no DMA size selection) and (b) sintered (spherical) silver particles, particle size is 28.5 nm based on DMA selection and 28.6 nm based on TEM measurement. TEM measurement is based on total of 139 particles. (Reprinted from Zhou and Zachariah 2011 with permission from Elsevier.)

charged particles were measured through a setup consisting of a NanoDMA and an Ultrafine Condensation Particle Counter (CPC TSI 3776; TSI Inc., St. Paul, MN, USA). Detailed information regarding the operation principles of the measurement setup and its applications can be found elsewhere (Knutson and Whitby 1975; Higgins et al. 2002; Zhou et al. 2008; Shrivastava et al. 2009).

The major advantage of this single DMA setup is its simplicity. Neutral particles are sent to the photoelectric ionization chamber without pre-size selection to ensure enough particle counts for electrical mobility measurements. Because the DMA only classifies charged particles, the mobility size distribution of photoelectric charged particle can be obtained directly. With the light source turned off, the particles are passed through a neutralizer which gives particles a known charge distribution, so that the true mobility size distribution of neutral particles can be obtained (as shown in Figure 2). Comparing the photoelectric ionized particle distribution to the neutral particle size distribution, the size-resolved particle charging efficiency can be obtained.

On the other hand, the drawback of this single DMA configuration as compared with standard tandem differential mobility

analysis (TDMA; Zhou et al. 2008) is the lack of capability to differentiate single- or multiple-particle charging state in the mobility spectrum. As the object of this work is to probe single charging from photoelectric ionization, we had to ensure that multiple charging states are minimized from photoelectric ionization charging. To ensure this constraint, we conducted TDMA experiments by adding an additional DMA followed by a neutralizer between the sintering furnace and the particle precipitator. In these experiments, the first DMA was held at a fixed voltage, and together with the neutralizer and the particle precipitator, the system functions as a monodispersed neutral particle source. With this experiment the photoelectric charging states could be directly evaluated. The TDMA experiments, for which we only summarize the results, were conducted for 30 and 60 nm aggregates particles. With the output slit of the monochromator fully open, the system operates at a photon-rich condition and significant double and even triple particle charging states were observed. As we reduced the slit width, multiple charging states first diminished followed by a decrease in the singly charged particles. For our subsequent charging experiments, we operated the UV source and monochromator such that the bandpass was between 0.7 and 3 nm (energy bandpass between 0.09 to 0.02 eV) depending on wavelength to ensure primarily single charging conditions.

It has been reported previously that aerosol photocharging is usually accompanied by simultaneous diffusion discharging, and the effect of diffusion discharging can be significant when highly concentrated particles are illuminated by intense UV radiation (Maisels et al. 2003). It is thus possible that at the particle concentrations employed in this work (Figure 2), diffusion discharging cannot be ignored. However, a direct comparison of the results by Maisels et al. with this work may not be appropriate, as the experiments were carried out at distinctively different conditions. In Maisels et al.'s work, a much more powerful UV irradiation source was used which can result in particle charge states of  $\sim +10$ . On the other hand, we operated our experiments at a low photon energy and low irradiation condition so that negative ions concentrations should be significantly lower than the previous work. Despite this, it is still possible that diffusion discharging may still be important due to the enhancement factor in the collision rate between a gas-ion and a particle of oppositely charge. To assess the importance of diffusion discharging, we conducted standard TDMA experiments and measured the particle photocharging efficiency under low particle concentration conditions  $\sim 10^3$  #/cc. These TDMA measurements showed that UV charging efficiencies are consistent with our simplified single DMA method, and we concluded that the diffusion discharging can be safely ignored in this work. The comparison of TDMA and single DMA results can be found in the online supplementary information.

## 2.2. Data Interpretation

The main objective of this work is to understand the charging dynamics of metal nanoparticles under UV irradiation. The

photoelectric ionization of particles suspended in gas has been investigated in several studies (Schmidt-Ott et al. 1980; Schleicher et al. 1993; Matter et al. 1995; Maisels et al. 2002). Generally speaking, a complete description of particle photoelectric charging includes photon absorption by the particle, electron escape over the potential barrier (photothreshold, image, and coulomb), and escape from particle-electron recombination by back-diffusion (Fowler 1931; Burtscher et al. 1982). In our study of nanoparticle photoelectric charging, the photoelectrical particle charging efficiency ( $CE$ ) was measured against particle mobility. Taking into account the fixed irradiation time and the single charging condition in our experiments, the measured particle charging efficiency ( $CE$ ) is proportional to the particle photoelectric yield,

$$y_{\text{particle}} \propto \frac{CE}{I}, \quad [1]$$

here  $I$  is the irradiation photon flux and  $y_{\text{particle}}$  denotes the particle photoelectric yield, defined as the number of emitted photoelectrons per incident photon per particle. From a practical point of view,  $y_{\text{particle}}$  is the most useful characteristic for particle charging, as it expresses the efficiency for a particle to acquire charge from UV irradiation. On the other hand from a fundamental prospective, it is the photoelectric quantum yield  $Y(h\nu)$  which provides insight into the charging dynamics. The photoelectric quantum yield  $Y(h\nu)$  is defined as the number of emitted photoelectrons per incident photon, per unit photon absorption cross section. The relation between the particle yield and the quantum yield is

$$y_{\text{particle}} \propto \sigma_{\text{abs}} Y(h\nu). \quad [2]$$

Therefore the quantum yield is also the total escape probability of electrons, from potential barriers and back-diffusion. The particle absorption cross section  $\sigma_{\text{abs}}$  is a function of particle size and incident light wavelength, as well as the particle's optical properties and is given by

$$\sigma_{\text{abs}} = Q_{\text{abs}} \times S_p, \quad [3]$$

where  $Q_{\text{abs}}$  is the particle optical absorption efficiency and  $S_p$  is the particle geometrical cross section. Thus, the quantum yield can be related to the measured charging efficiency as

$$\frac{CE}{I} \propto \sigma_{\text{abs}} Y(h\nu). \quad [4]$$

The behavior of the quantum yield  $Y(h\nu)$  from flat surfaces is believed to follow the well-known three-steps model by Berglund and Spicer (1964a,b), which has been extended to the case of spherical particles (Burtscher et al. 1982; Chen and Bates 1986; Muller et al. 1988). In the vicinity of the photoelectric ionization threshold (the Fowler-Nordheim limit  $h\nu - \Phi \leq \sim 1.5$  eV),

the quantum yield  $Y(h\nu)$  should follow the Fowler–Nordheim law (Fowler 1931)

$$Y(h\nu) = c(h\nu - \Phi)^m \quad [5]$$

where  $c$  is the material dependent photoelectric ionization constant and  $m = 2$  for metals. It has been confirmed experimentally that the Fowler–Nordheim law is also valid for small particles, where the photoelectric constant,  $c$ , becomes size dependent and significantly enhanced compared with a macroscopic surface (Schmidt-Ott et al. 1980; Burtscher et al. 1982). In our previous article, we have obtained the particle work function for both spheres and aggregates (Zhou and Zachariah 2011). With a knowledge of the particle work function, the evaluation of the photoelectric constant,  $c$ , becomes trivial once we know the quantum yield, therefore our discussion in this work will be focused on the quantum yield. For spheres, the data analysis is straightforward, since we can apply Mie theory directly to calculate the absorption cross section  $\sigma_{\text{abs}}$ , and the particle photoelectric quantum yield can be obtained from Equation (4). However, the problem for aggregates is more complicated, as there is no direct way to determine the photon absorption cross section of aggregates. One approach to estimate the total absorption cross section of the aggregates is by summing over the set of primary particle absorption cross sections. In this approximation known as the Rayleigh–Debye–Gans (RDG) model, interactions between primaries are not considered and absorption is treated as being independent of agglomerate morphology:

$$\sigma_{\text{abs,aggregate}} = N_p \sigma_{\text{abs,primary}}, \quad [6]$$

where  $N_p$  is the total number of primary particles within the aggregate. The validation of the RDG model using the more rigorous multiple sphere T-matrix model (Mackowski 1994) and methods to determine number of primary particles within aggregates from mobility measurements (Shin et al. 2009; Sorensen 2011) are discussed in the online supplementary information.

The RDG model suggests that an aggregate is equivalent to  $N_p$  individual primary spheres in terms of photon absorption. If we further assume the interactions between excited electrons and other primary particles or interactions between primary particles have no effect on an electrons escape probability, we can further construct an “ideal aggregate” such that not only the photon absorption, but also the quantum yield  $Y(h\nu)$  of aggregates is determined by the primary particle. In other words, the charging efficiency of an “ideal aggregate” would be independent of aggregate structure and is completely defined by its primary particles. This leads to relationship (7) for an “ideal aggregate”

$$\left(\frac{CE}{I}\right)_{\text{ideal aggregate}} = N_p \left(\frac{CE}{I}\right)_{\text{primary}}. \quad [7]$$

We can now evaluate the effect of aggregate structure by comparing the experimentally measured aggregates  $CE$  with the

“ideal charging efficiency,” by defining an aggregate structure factor,  $\chi$ ,

$$\chi = \frac{\left(\frac{CE}{I}\right)_{\text{aggregate}}}{N_p \left(\frac{CE}{I}\right)_{\text{primary}}}. \quad [8]$$

For our purposes, the  $CE$  of the primary particle is obtained by using the  $CE$  results for an isolated spherical particle whose size is equivalent to the primary particle size in aggregates. In this way, Equation (8) is entirely based on experimental measurement. The ratio  $\chi$  can be used as an indicator for an aggregate structure effect on the quantum yield (it is in fact the normalized quantum yield  $Y(h\nu)$ ), and it will be shown in our data analysis that  $\chi$  deviates from unity significantly as aggregates size increases, which suggests that aggregate structure does affect charging dynamics. Note that this “ideal aggregate” is related to the electron emission process and not “ideal” in the context of electrical mobility.

### 2.3. Particle Yield Versus Friction Coefficient

Keller et al. (2001) demonstrated that particle photoelectric yield  $y_{\text{particle}}$  is proportional to the particle frictional coefficient  $f_d$  and thus inversely proportional to particle mobility  $Z$

$$y_{\text{particle}} \propto \frac{CE}{I} \propto f_d \propto \frac{1}{Z}, \quad [9]$$

which can give us

$$Y(h\nu) \propto \frac{f_d}{\sigma_{\text{abs}}}. \quad [10]$$

In principle, Equations (9) and (10) enable one to access quantum yield directly from particle mobility without actually conducting a photoelectric charging measurement. Based on the scaling law, for spherical particles in the free molecular regime, since the frictional cross section is proportional to the square of the mobility diameter,  $D_m^2$ , and the photon absorption cross section is proportional to  $D_m^3$ , we can expect the quantum yield  $Y(h\nu)$  of spherical particles to have a  $D_m^{-1}$  dependence. For aggregates, the quantum yield should follow  $D_m^{-0.30}$  dependence (see the online supplementary information). These scaling-laws-based “theoretical dependence” are summarized in Table 1.

In this work, the scaling law between particle photoelectric yield  $y_{\text{particle}}$  and the particle frictional coefficient  $f_d$  was evaluated using our experimental data, and the above “theoretical dependence” of quantum yield was also compared with our experimentally measured quantum yield obtained from Equation (4).

## 3. RESULTS AND DISCUSSION

In our experiments, monochromatic UV light in the wavelength range between 200 and 280 nm (incident photon energies from 6.20 to 4.43 eV, energy bandpass from 0.09 to 0.02 eV depending on wavelength selected) was selected with

TABLE 1  
Mobility size dependence of quantum yield

	Based on scaling law (Equation (10))	Based on charging efficiency measurement (Figures 6 and 7)
Spheres	$D_m^{-1}$	$D_m^{-1.03}$
Aggregates	$D_m^{-0.30}$	$D_m^{-0.28}$
Ideal aggregates	$d_p^{-1}$ (constant, independent of $D_m$ )	

$D_m$  is mobility size;  $d_p$  is primary particle size. At a given particle growth condition, the aggregates consisted of primary particles of the same  $d_p$

the monochromator. The mobility spectrum of photoelectric ionized particle at each incident photon energy as well as the PMT measured relative light intensity was obtained.

The normalized charging efficiency  $CE/I$  as the function of mobility size is shown in Figure 4a and b for spherical and aggregate-

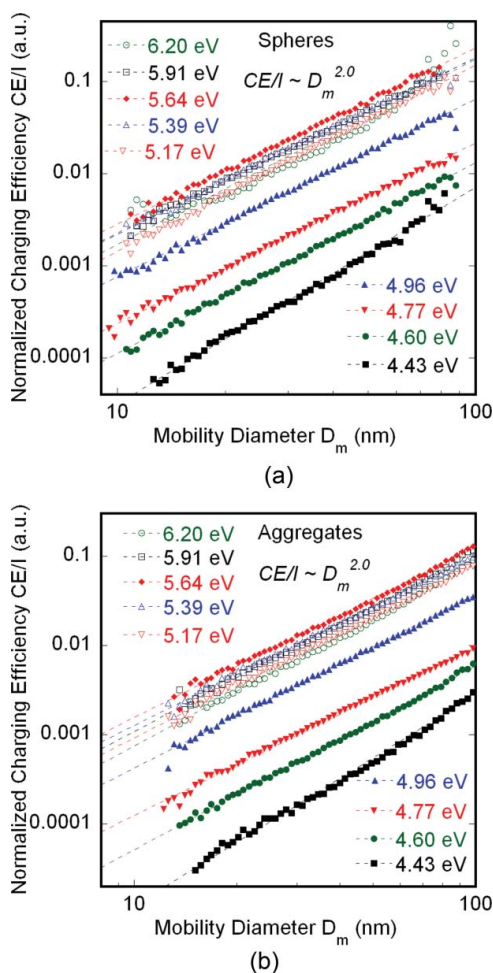


FIG. 4. Size-resolved normalized charging efficiency for (a) spherical silver particles and (b) aggregate silver particles. Dotted lines are power law fits. (Color figure available online.)

gated silver particles, respectively. As expected, the photoelectric charging efficiency shows a strong size dependence as well as incident photon energy dependence. In general, larger sizes and higher photon energies lead to greater charging; however, as the photon energy further increases above the Fowler–Nordheim limit, the charging efficiency decreases, and this behavior is discussed in our previous work (Zhou and Zachariah 2011). Here each normalized  $CE/I$  was fitted with a power function to determine its dependence on mobility size  $D_m$ , which are shown in Figure 4a and b as the dotted curves. Since all curves have the same shape regardless of photon energy, we obtain an average of the normalized charging efficiency  $CE/I \propto D_m^{2.0}$  for both spheres and aggregates.

As the particle charging dynamics is a manifestation of combined effects of light absorption cross section  $\sigma_{\text{abs}}$ , and electron escaping processes represented by the quantum yield  $Y(h\nu)$ , our first task is to compare the general behavior of the photon absorption cross section of spheres and aggregates. The particle photon absorption cross sections as a function of particle mobility size are plotted in Figure 5, for both spheres and aggregates. The cross sections of spheres were calculated directly from Mie theory, and the cross sections of aggregates were calculated assuming a primary particle size of 15 nm. The calculation was performed for all photon energies, but only selected results were used to show the general trend. First we can see that spheres show less incident light dependence than aggregates in the wavelength range investigated in this study (200–280 nm). From a photon absorption process point of view, it is more important to compare the cross section between spheres and aggregates. According to Mie theory calculations, the photon absorption cross section of spherical particles in the thin optical limit is proportional to particle mass ( $\sigma_{\text{abs}} \propto D_m^3$ ). Similarly, the photon absorption cross section of aggregates is also proportional to particle mass based on the RDG assumption (Equation 6). Thus, spheres and aggregates should have the same photon

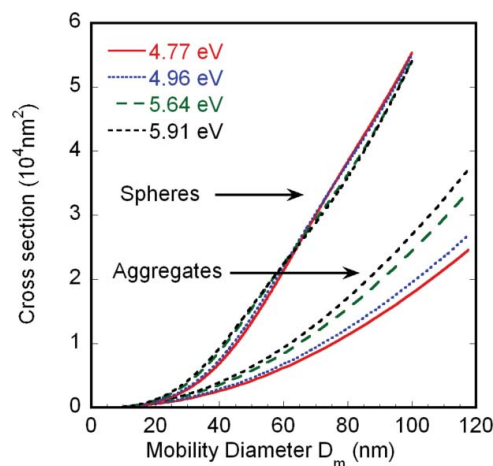


FIG. 5. Calculated photon absorption cross sections for spheres and aggregates as a function of particle mobility size. (Color figure available online.)

absorption on a mass basis. However, if we compare particles of the same mobility, the absorption cross section calculation results, Figure 5, shows that the cross sections of aggregates are significantly smaller than spheres because aggregates have smaller mass than spheres of the same mobility. Thus, a spherical particle can absorb light more efficiently than an aggregate of the same mobility size. For instance, Figure 5 suggests that the photon absorption of an 80 nm aggregate particle is only about 30% of an 80 nm sphere.

Using the calculated light absorption cross sections, we are in the position to evaluate the quantum yield of spheres using Equation (4). Results at selected incident photon energy are shown in Figure 6, where the data are normalized to 15-nm particles. As we can see from Figure 6, the quantum yield  $Y(h\nu)$  is approximately constant and size independent for particles 50 nm or larger, and we would expect it to be close to the value of a flat surface. As particle size decreases into the free molecular regime, the quantum yield increases significantly. For example, at photon energy of 5.17 eV, as particle size decreased from 15-nm particle to 10 nm, an enhancement factor of  $\sim 2$  is observed. This enhancement behavior is consistent with previous work where enormous photoelectric activities of ultrafine particles are observed for particles less than  $\sim 10$  nm as compared with bulk surfaces (Schmidt-Ott et al. 1980), and also agrees with a reported enhancement factor of  $\sim 2$  for silver as particle size changed from 15 to 6 nm (Jiang et al. 2007). The particle size dependence of quantum yield was obtained by curve fitting the data in the small size range (free-molecular regime), from which a power law dependence for selected incident photon energy is also shown in Figure 6. On average, the measured quantum yield  $Y(h\nu)$  follows a  $\propto D_m^{-1.03}$  dependence. This result is listed in Table 1 and is in excellent agreement with the “theoretical dependence” of  $\propto D_m^{-1}$ .

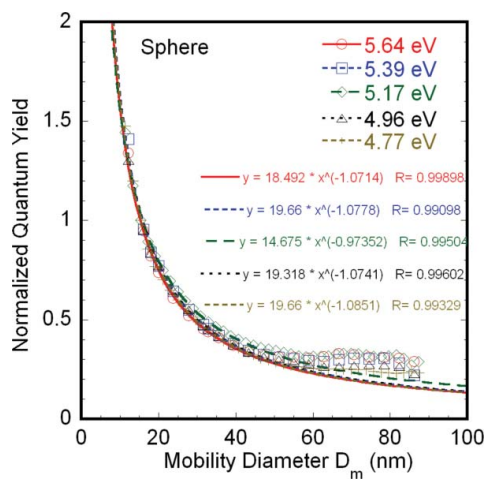


FIG. 6. Measured quantum yield for spherical particles. Data normalized with respect to a 15 nm sphere. The particle size dependence of quantum yield was obtained by curve fitting the data in the small size range (free molecular regime). (Color figure available online.)

In our previous work (Zhou and Zachariah 2011), we demonstrated that the native particle work function of aggregates is determined by its primary particle size, not its mobility size. Following the same logic, one may consider if the photoelectric charging dynamics of aggregates is also solely defined by the primary particle. To test this hypothesis, we evaluated the aggregates  $CE$  against the “ideal aggregates” using Equation (8), with selected results plotted in Figure 7. For small aggregates, the particle structure is proximate to spheres, so that the  $\chi$  approaches unity. This fact indicates that the primary particle does determine the aggregate charging dynamics to certain extent. However, the ratio  $\chi$ , as seen from Figure 7, is aggregate mobility size dependent, which indicates that the structure of aggregates plays a role in aggregate charging dynamics. It is thus clear that even though the native work function of aggregates is determined by the primary particle size, the charging dynamics is not just simply a summation of individual primary particles and cannot be modeled as the “ideal aggregate.” As mentioned earlier, the ratio  $\chi$  is also the normalized quantum yield, which when fitted to a power law is shown as the dotted lines in Figure 7. The averaged power law dependence obtained is  $\propto D_m^{-0.28}$  as listed in Table 1. This observed size dependence, is also consistent to the scaling-law-based “theoretical dependence” of  $\propto D_m^{-0.30}$ . Since the data presented in Figures 6 and 7 are normalized to 15 nm spheres, they can be compared with each other directly. The quantum yield of both spheres and aggregates (also expressed as  $\chi$ , for aggregates) shows a decreasing trend with increasing particle mobility size. However, the quantum yield for spheres shows a rapid decline and approaches a constant value, while the drop of the quantum yield (factor  $\chi$ ) for aggregates has a more moderate decline. As a result, aggregates show much higher quantum yield than spheres of the same mobility size over a broad range of particle size. For example, the

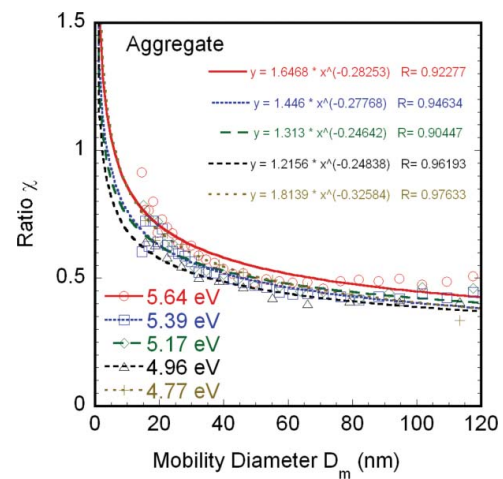


FIG. 7.  $\chi$  as function of particle mobility size. Here,  $\chi$  is the ratio of experimentally measured aggregates  $CE$  with the “ideal charging efficiency” defined in Equation (12) which is also the quantum yield  $Y(h\nu)$  normalized to a 15 nm sphere. (Color figure available online.)

normalized yield of 60 nm aggregate is about 0.5 while a 60 nm sphere is only 0.25. However, as we have seen in Figure 5, the aggregates can absorb light less efficiently than spheres (for the same mobility size), and hence the advantage of higher quantum yield of aggregates is offset with low absorption efficiency. As we will show later, the overall charging efficiency of aggregates is in fact lower than spheres.

As Table 1 indicated, our measured mobility size dependence of quantum yield corroborates the scaling-law-based “theoretical dependence,” for both spheres and aggregates. To further evaluate the scaling law, we turn our attention to the relationship between charging efficiency and particle mobility. A plot of all of experimental data at each incident photon energy is hard to read, so we only show selected results in Figure 8a and b for spheres and aggregates, respectively.

There is a clear linear relationship between the normalized charging efficiencies, and  $1/Z$  for both spheres and aggregates

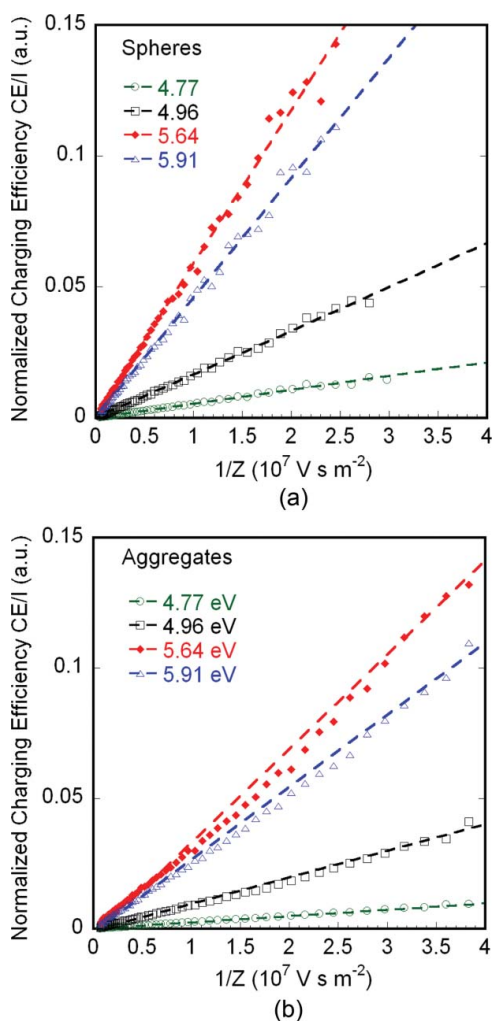


FIG. 8. Normalized charging efficiency vs.  $1/Z$  for (a) spheres and (b) aggregates. Dashed line is linear fit using data points in full size range 10–100 nm, dotted line only uses data points in size range  $\leq 40$  nm. (Color figure available online.)

in the mobility size range 10–100 nm. This linear relationship appears to hold not only in the Fowler–Nordheim regime ( $h\nu - \Phi \leq \sim 1.5$  eV), but over the full range of incident photon energies explored (e.g., 5.91 eV). The slight scatter in the data at low mobility is likely due to the low particle counts resulting from being in the tail of the particle size distribution, as shown in Figure 2. Figure 8a and b support the previously reported scaling law for spheres as well as aggregates, that the charging efficiency is proportional to the particle friction coefficient  $f_d$  (Equation (8)). The particle friction coefficient  $f_d$  represents the energy/momentum transfer between gas molecules and the particle surface. If the process of gas molecules impinging on the particle surface and scattering from the surface occurred with the same primary particle size dependence as photon absorption by a particle and subsequent electron escape, the scaling law should hold. Since the frictional surface area is proportional to  $D_m^2$ , the excellent linear fit in Figure 8a and b is also consistent with the  $CE/I \propto D_m^{2.0}$  relation we obtained from Figure 4a and b.

Finally, we are in the position to compare the charging efficiency of spheres and aggregates. As mentioned earlier, spherical particles can absorb light more efficiently than an aggregate of the same mobility, but aggregates have a higher quantum yield. From Figure 8a and b, we can see the  $CE/I$  of spheres are significantly higher than aggregates at the same incident photon energy. Previous work suggested that the scaling law proportionality constant (the slopes in Figure 8a and b) is independent of particle morphology (Keller et al. 2001). This argument would suggest that particles of the same mobility, regardless of their structure, should have the same charging efficiency. Our results contradict the previous study, and this is more clearly seen in Figure 9 which plots the charging efficiency ratios of aggregate over spheres for each incident photon energy as a function of particle mobility size. Most of the measured aggregate/sphere ratios fall between 0.4 and 0.8. The charging efficiency ratios of aggregates over spheres were also analyzed in the mass basis. The aggregate data are converted to mass basis through

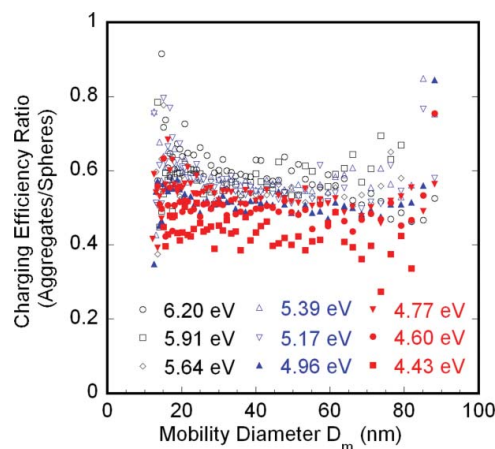


FIG. 9. Charging efficiency ratio for aggregates over spheres as a function of mobility size. (Color figure available online.)

Equation (9), and assuming the mobility sizes of spheres are also their mass sizes, we found the aggregates can be charged more efficiently by factor of 1.1–1.5 than spheres of the same mass. This calculation was confirmed through another approach by going back to the PSD of neutral sintered and aggregated particles. Upon sintering, the peak size shifted from 39 nm to 27 nm, and if we assume they have the same mass, the ratio can be calculated which is in the range of 1.1–1.5 depending on the wavelength.

#### 4. CONCLUSION

The wavelength-selected UV charging dynamics of structure-controlled nanoparticles was studied by ion mobility separation. The observed particle charging efficiency of spheres is proportional to particle frictional coefficient, which is in excellent agreement with the previously reported scaling law. In order to investigate particle UV charging behavior in detail, we performed photon absorption cross-section calculations and extracted the photoelectric quantum yield for spheres and aggregates. Even though the aggregates have higher quantum yield than a sphere of the same mobility size, the overall charging efficiency of spheres is higher due to their larger photon absorption cross sections. The quantum yield of spherical particles is significantly enhanced as particle size decreases, and shows a  $D_m^{-1}$  dependence in the free molecular regime. For aggregates, although the native particle work function is solely defined by the primary particle size, the photoelectric quantum yield follows  $D_m^{-2.8}$  dependence, which suggests the structure of aggregates also plays a role in aggregate charging dynamics. The charging dynamics is not just simply a summation of individual primary particles, and cannot be modeled as the “ideal aggregate.”

#### REFERENCES

- Berglund, C. N., and Spicer, W. E. (1964a). Photoemission Studies of Copper and Silver: Experiment. *Phys. Rev.*, 136(4A):A1044.
- Berglund, C. N., and Spicer, W. E. (1964b). Photoemission Studies of Copper and Silver: Theory. *Phys. Rev.*, 136(4A):A1030.
- Burtscher, H., Scherrer, L., Siegmann, H. C., Schmidt-Ott, A., and Federer, B. (1982). Probing Aerosols by Photoelectric Charging. *J. Appl. Phys.*, 53(5):3787–3791.
- Chen, Q. Y., and Bates, C. W. (1986). Geometrical Factors in Enhanced Photoyield from Small Metal Particles. *Phys. Rev. Lett.*, 57(21):2737–2740.
- Fowler, R. H. (1931). The Analysis of Photoelectric Sensitivity Curves for Clean Metals at Various Temperatures. *Phys. Rev.*, 38(1):45.
- Fuchs, N. A. (1963). On the Stationary Charge Distribution on Aerosol Particles in a Bipolar Ionic Atmosphere. *Pure Appl. Geophys.*, 56(1):185–193.
- Higgins, K. J., Jung, H. J., Kittelson, D. B., Roberts, J. T., and Zachariah, M. R. (2002). Size-Selected Nanoparticle Chemistry: Kinetics of Soot Oxidation. *J. Phys. Chem. A*, 106(1):96–103.
- Hontanon, E., and Kruijs, F. E. (2008). Single Charging of Nanoparticles by UV Photoionization at High Flow Rates. *Aerosol Sci. Technol.*, 42(4):310–323.
- Jiang, J. K., Hogan, C. J., Chen, D.-R., and Biswas, P. (2007). Aerosol Charging and Capture in the Nanoparticle Size Range (6–15 nm) by Direct Photoionization and Diffusion Mechanisms. *J. Appl. Phys.*, 102(3):034904.
- Jung, H., and Kittelson, D. B. (2005). Characterization of Aerosol Surface Instruments in Transition Regime. *Aerosol Sci. Technol.*, 39(9):902–911.
- Keller, A., Fierz, M., Siegmann, K., Siegmann, H. C., and Filippov, A. (2001). Surface Science with Nanosized Particles in a Carrier Gas. *J. Vac. Sci. Technol. A*, 19(1):1–8.
- Knutson, E. O., and Whitby, K. T. (1975). Aerosol Classification by Electric Mobility: Apparatus, Theory, and Applications. *J. Aerosol. Sci.*, 6(6):443–451.
- Lall, A. A., Seipenbusch, M., Rong, W., and Friedlander, S. K. (2006). On-Line Measurement of Ultrafine Aggregate Surface Area and Volume Distributions by Electrical Mobility Analysis: II. Comparison of Measurements and Theory. *J. Aerosol Sci.*, 37(3):272–282.
- Mackowski, D. W. (1994). Calculation of Total Cross-Sections of Multiple-Sphere Clusters. *J. Opt. Soc. Am. A*, 11(11):2851–2861.
- Maisels, A., Jordan, F., and Fissan, H. (2002). Dynamics of the Aerosol Particle Photocharging Process. *J. Appl. Phys.*, 91(5):3377–3383.
- Maisels, A., Jordan, F., and Fissan, H. (2003). On the Effect of Charge Recombination on the Aerosol Charge Distribution in Photocharging Systems. *J. Aerosol Sci.*, 34(1):117–132.
- Matter, D., Mohr, M., Fendel, W., Schmidt-Ott, A., and Burtscher, H. (1995). Multiple Wavelength Aerosol Photoemission by Excimer Lamps. *J. Aerosol Sci.*, 26(7):1101–1115.
- Muller, U., Burtscher, H., and Schmidt-Ott, A. (1988). Photoemission from Small Metal Spheres—A Model Calculation Using an Enhanced 3-Step Model. *Phys. Rev. B*, 38(11):7814–7816.
- Oh, H., Park, H., and Kim, S. (2004). Effects of Particle Shape on the Unipolar Diffusion Charging of Nonspherical Particles. *Aerosol Sci. Technol.*, 38(11):1045–1053.
- Reiners, T., and Haberland, H. (1996). Plasmon Enhanced Electron and Atom Emission from a Spherical Sodium Cluster: Na-91(-). *Phys. Rev. Lett.*, 77(12):2440–2443.
- Schleicher, B., Burtscher, H., and Siegmann, H. C. (1993). Photoelectric Quantum Yield of Nanometer Metal Particles. *Appl. Phys. Lett.*, 63(9):1191–1193.
- Schmidt-Ott, A., Schurtenberger, P., and Siegmann, H. C. (1980). Enormous Yield of Photoelectrons from Small Particles. *Phys. Rev. Lett.*, 45(15):1284–1287.
- Shimada, M., Cho, S. J., Okuyama, K., Tamura, T., Adachi, M., and Fujii, T. (1997). Removal of Airborne Particles by a Tubular Particle Removal Device Using UV/Photoelectron Method. *J. Aerosol Sci.*, 28(4):649–661.
- Shin, W. G., Mulholland, G. W., Kim, S. C., Wang, J., Emery, M. S., and Pui, D. Y. H. (2009). Friction Coefficient and Mass of Silver Agglomerates in the Transition Regime. *J. Aerosol Sci.*, 40(7):573–587.
- Shin, W. G., Wang, J., Mertler, M., Sachweh, B., Fissan, H., and Pui, D. Y. H. (2010). The Effect of Particle Morphology on Unipolar Diffusion Charging of Nanoparticle Agglomerates in the Transition Regime. *J. Aerosol Sci.*, 41(11):975–986.
- Shrivastava, M., Gidwani, A., and Jung, H. S. (2009). Modeling Oxidation of Soot Particles Within a Laminar Aerosol Flow Reactor Using Computational Fluid Dynamics. *Aerosol Sci. Technol.*, 43(12):1218–1229.
- Sorensen, C. M. (2011). The Mobility of Fractal Aggregates: A Review. *Aerosol Sci. Technol.*, 45:765–779.
- Tsai, D. H., Kim, S. H., Corrigan, T. D., Phaneuf, R. J., and Zachariah, M. R. (2005). Electrostatic-Directed Deposition of Nanoparticles on a Field Generating Substrate. *Nanotechnology*, 16(9):1856–1862.
- Weber, A. P., Seipenbusch, M., and Kasper, G. (2001). Application of Aerosol Techniques to Study the Catalytic Formation of Methane on Gasborne Nickel Nanoparticles. *J. Phys. Chem. A*, 105(39):8958–8963.
- Wong, K., Kasperovich, C., Tikhonov, G., and Kresin, V. V. (2001). Photoionization Efficiency Curves of Alkali Nanoclusters in a Beam and Determination of Metal Work Functions. *Appl. Phys. B-Lasers. O.*, 73(4):407–410.
- Wood, D. M. (1981). Classical Size Dependence of the Work Function of Small Metallic Spheres. *Phys. Rev. Lett.*, 46(11):749–749.
- Zhou, L., Rai, A., Piekielek, N., Ma, X., and Zachariah, M. R. (2008). Ion-Mobility Spectrometry of Nickel Nanoparticle Oxidation Kinetics: Application to Energetic Materials. *J. Phys. Chem. C*, 112:16209–16218.
- Zhou, L., and Zachariah, M. R. (2012). Size Resolved Work Function Measurement of Free Nanoparticles: Aggregates vs. Spheres. *Chem. Phys. Lett.*, 525–526:77–81.